THE JOURNAL OF PHYSICAL CHEMISTRY C

Article

pubs.acs.org/JPCC

High Open Circuit Voltage in Sb_2S_3/Metal Oxide-Based Solar Cells

Tzofia Englman, Eyal Terkieltaub, and Lioz Etgar*

Institute of Chemistry, Casali Center for Applied Chemistry, The Hebrew University of Jerusalem, Jerusalem 91904, Israel

ABSTRACT: This paper presents for the first time Sb_2S_3-based solar cells operating on scaffold film. The scaffolds studied are Al_2O_3 and ZrO_2, for which no electron injection from the Sb_2S_3 to the Al_2O_3 or ZrO_2 is possible. As a result, one of the highest open circuit voltages (V_{oc}) of 0.712 V was observed for this solar cell configuration. Electron dispersive spectroscopy (EDS) was performed, revealing complete pore filling of the Sb_2S_3 into the metal oxide pores (e.g., Al_2O_3 or ZrO_2); the complete pore filling of the Sb_2S_3 is responsible for the photovoltaic performance (PV) of this unique solar cell structure. In addition, intensity modulated photovoltage and photocurrent spectroscopy (IMVS and IMPS) were performed to extract the electron diffusion length. Electron diffusion length in the range of 900 nm to 290 nm (depending on the light intensity) was observed, which further supports the operation of metal oxide/Sb_2S_3 solar cell configuration. Moreover, the Al_2O_3-based cells have longer electron diffusion length than the TiO_2-based cells, supporting the higher open circuit voltage of the noninjected metal oxide-based cells. This work demonstrates the potential of Sb_2S_3 to gain high voltage and to perform on a scaffold substrate without requiring electron injection.

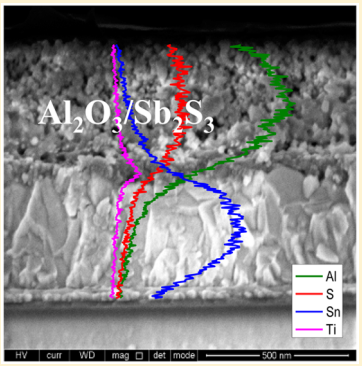

INTRODUCTION

Dye-sensitized solar cells (DSSCs) are low-cost alternatives to conventional solar cells.

In these cells, the photoexcited dye injects electrons into the conduction band of TiO_2, and then the oxidized dye is neutralized by electron donation from an electrolyte, or the counter-charge is extracted by an organic solid-state hole transport. The overall efficiency and long-term stability of DSSCs are major issues, investigated by numerous laboratories, exploring various sensitizers, photoanode materials, counter electrodes, and redox systems.[1−9]

Using solid-state hole transport material (HTM) makes DSSCs more attractive than liquid DSSCs since leakage problems in liquid DSSCs pose difficulties in commercialization of these solar cells. However, problems still arise in regard to the stability of these solar cells because of the dye, which consists of organic molecules. An alternative is to replace the organic dye molecules with inorganic semiconductors that can be used as light harvesters (and sensitizers, in some cases) in the solar cell, among them semiconductor quantum dots (QDs),[10,11] extremely thin absorbers (such as Sb_2S_3),[12,13] and recently, organo-metal perovskite.[14,15]

Sb_2S_3 is semiconductor material with a band gap of 1.7−1.8 eV, high absorption coefficient (1.8×10^5 cm^{-1} at 450 nm), high stability in air,[16] and nontoxic characteristics, which makes it suitable for use as a light harvester in solar cells.

Sb_2S_3-based solar cells have been investigated using several HTMs, e.g., CuSCN,[17] spiro-MeOTAD,[13] poly-3-hexylthiophene (P3HT),[12] phenyl-C_{61}-butyric acid methyl ester (PCBM), and poly[2,6-(4,4-bis-(2-ethylhexyl)-4H-cyclopenta [2,1-b;3,4-b′]dithiophene)-alt-4,7(2,1,3-benzothiadiazole)] (PCPDTBT),[18] all of which increase the power conversion efficiency. In the case of PCPDTBT[18] as the HTM, power conversion efficiency of 6.3% was achieved, due to chemical interactions between the Sb_2S_3 and the PCPDTBT.

Moreover, surface treatment of the Sb_2S_3 was proved to increase the PV parameters. Decyl phosphine acid (DPA) was demonstrated as increasing the open circuit voltage (V_{oc}) from 0.47 to 0.51 V.[16] The DPA molecules are attached to the surface of the TiO_2 which is not covered by the Sb_2S_3, resulting in the decrease of the recombination. Mg^{2+}, Ba^{2+}, and Al^{3+} were demonstrated to enhance the power conversion efficiency, achieving 4.1% by forming a blocking layer at the interface of the TiO_2 and the Sb_2S_3 which reduces the recombination.[19] Recently Seok et al. reported a high efficiency of 7.5%[20] using a treatment of sulfurization with thioacetamide Sb_2S_3 film. The high power conversion efficiency can be attributed to the extinction of trap sites in the Sb_2S_3.

The current Sb_2S_3-based solar cell structure demands a higher conduction band of the Sb_2S_3 than the metal oxide conduction band (e.g., TiO_2, ZnO) for electron injection from the Sb_2S_3 to the metal oxide. Recently, organo metal halide perovskite solar cells have demonstrated the potential to work with Al_2O_3 which functions as a scaffold in the solar cell.[21] No electron injection is possible in this perovskite solar cell structure. In this work, we demonstrate for the first time that Sb_2S_3 can function with Al_2O_3 or ZrO_2 as a scaffold in the solar cell. Due to the higher conduction band of the Al_2O_3 or the ZrO_2 electron injection is not possible. Moreover, high open circuit voltage of 0.712 V is obtained in the ZrO_2/Sb_2S_3 solar cell structure. Electron dispersive spectroscopy (EDS) was performed to reveal complete pore filling of the Sb_2S_3 into the

Received: May 3, 2015
Revised: May 20, 2015
Published: May 21, 2015

DOI: 10.1021/acs.jpcc.5b04231
J. Phys. Chem. C 2015, 119, 12904−12909

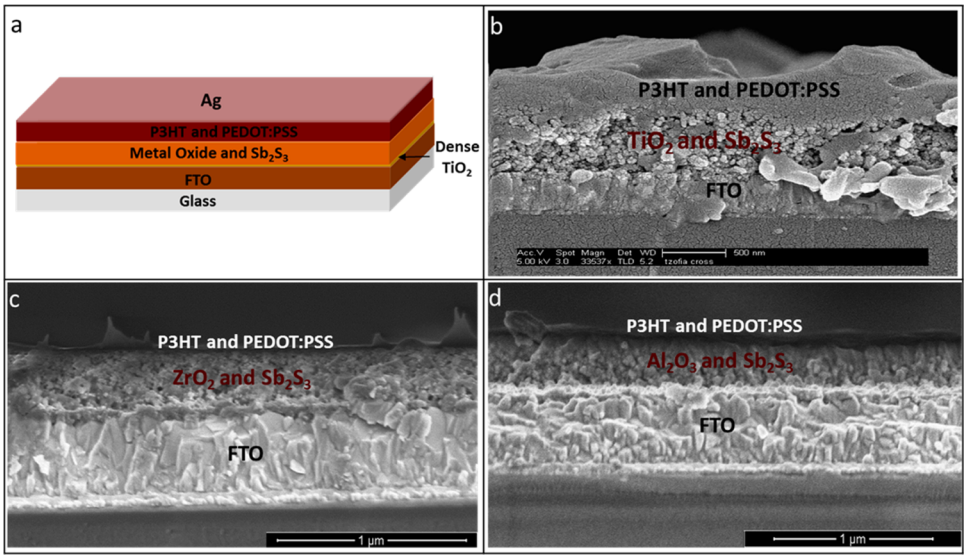

Figure 1. (a) Schematic illustration of the solar cell. SEM cross sections of (b) TiO_2/Sb_2S_3 solar cell, (c) ZrO_2 /Sb_2S_3 solar cell, and (d) Al_2O_3/Sb_2S_3 solar cell.

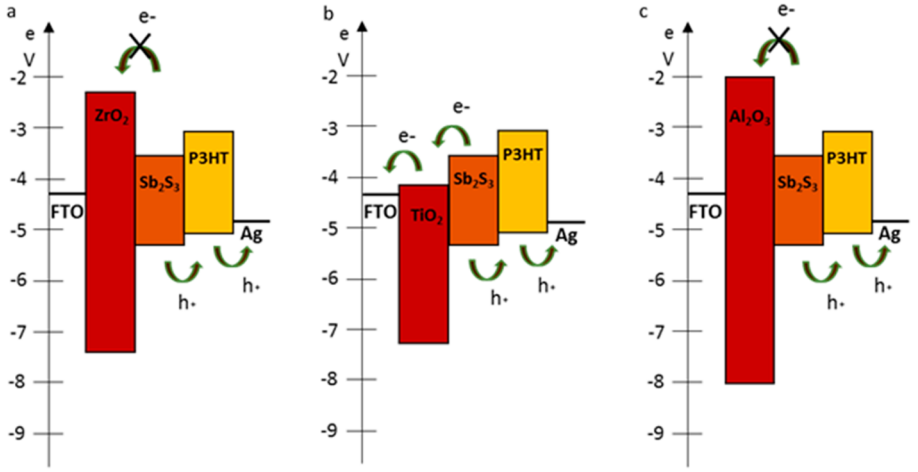

Figure 2. Energy band diagram of (a) ZrO_2/Sb_2S_3, (b) TiO_2/Sb_2S_3, and (c) Al_2O_3/Sb_2S_3 solar cells configurations. The energy level positions are according to refs 24 and 25.

metal oxide (e.g., Al_2O_3 or ZrO_2) pores; the complete pore filling of the Sb_2S_3 is responsible for the photovoltaic performance (PV) of this unique solar cell structure. Intensity modulated photovoltage and photocurrent spectroscopy (IMVS and IMPS) were performed to extract the electron diffusion length in the Sb_2S_3. Electron diffusion length in the range of 900 nm to 290 nm (depending on the light intensity) was observed.

RESULTS AND DISCUSSION

The structure of the Sb_2S_3-based solar cell is presented in Figure 1a, composed of FTO glass/TiO_2 compact layer/mesoporous metal oxide/Sb_2S_3/P3HT/PEDOT:PSS/silver. The Sb_2S_3 was deposited by the chemical bath deposition (CBD) method previously described.[17,22] In this work, three metal oxides were studied in combination with the Sb_2S_3 in the solar cell—TiO_2, Al_2O_3 and ZrO_2. Scanning electron microscopy (SEM) cross sections of the solar cells studied are presented in Figure 1b–d.

In the mesoporous TiO_2/Sb_2S_3 configuration, on illumination, electrons are injected into the mesoporous TiO_2 from the Sb_2S_3, which functions as a light harvester, while holes are transported to the HTM (P3HT/PEDOT:PSS) and to the silver contact as shown in Figure 2b. However, in the ZrO_2/Sb_2S_3 and the Al_2O_3/Sb_2S_3 solar cell configurations, the electron injection from Sb_2S_3 is not possible, as shown in Figure 2a,c, respectively.

O'Mahoney et al.[23] reported that charge injection is not possible at the ZrO_2/Sb_2S_3 interface; as a result, no solar cell PV performance was discernible. In the solar cell configurations shown in Figure 2a,c, the higher conduction band of the metal oxide compared to the Sb_2S_3 conduction band does not allow electron injection from the Sb_2S_3 to the metal oxide. Surprisingly, both solar cell structures have PV response with high V_{oc}. It is suggested that a complete pore filling of the Sb_2S_3 through the metal oxide film thickness is necessary for operation of the solar cell. Therefore, photogenerated charges are separated at the Sb_2S_3 layer (and not at the metal oxide/Sb_2S_3 interface) and transported to opposite contacts, FTO and P3HT.

Figure 3 presents the absorption spectra of the Sb_2S_3 layer measured on the different metal oxides; in all cases, the

DOI: 10.1021/acs.jpcc.5b04231
J. Phys. Chem. C 2015, 119, 12904–12909

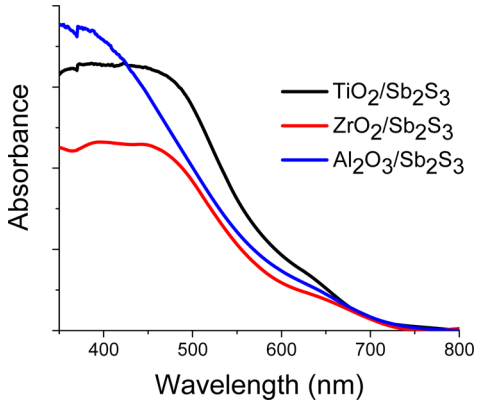

Figure 3. Absorption spectra of the Sb_2S_3 adsorbed on the metal oxides studied.

absorption onset agrees well with the band gap of the Sb_2S_3. Moreover, the slight red shift in the absorption spectra of the TiO_2 is related to the thicker TiO_2 mesoporous film compared to Al_2O_3 and ZrO_2 mesoporous films. In the case of the thicker mesoporous metal oxide film, more Sb_2S_3 can fill the pores, which results in the increase and red-shifted of the absorption, corresponding with the higher current density observed for the TiO_2-based cells.

Table 1. PV Parameters of the Solar Cells Studied

	J_{sc}(mA cm^{-2})	V_{oc} (V)	FF (%)	efficiency (%)
TiO_2/Sb_2S_3	10.6	0.504	58.8	3.24
Al_2O_3/Sb_2S_3	7.8	0.674	43.7	2.48
ZrO_2/Sb_2S_3	6.8	0.712	53.5	2.64

Table 1 and Figure 4a show the photovoltaic parameters and the current voltage curves for the different solar cells fabricated on the metal oxides. The TiO_2-based cells show better efficiencies than the Al_2O_3- and ZrO_2-based cells, mainly due to the higher current density observed in these cells. However, the Al_2O_3- and ZrO_2-based cells demonstrate higher V_{oc} than the TiO_2-based cells. V_{oc} of 0.712 V was observed for the ZrO_2-based cells, and V_{oc} of 0.5 V was observed for the TiO_2-based cells. V_{oc} of 0.712 V achieved for the ZrO_2-based cells is one of the highest demonstrated for Sb_2S_3 thin film solar cells. Typical open circuit voltage in Sb_2S_3-based solar cells is in the range of 500−630 mV.[12,16,18,19]

It can be argued that due to the difference in the solar cells structures, when electron injection is not permitted, as in the case of Al_2O_3/ Sb_2S_3 and ZrO_2/ Sb_2S_3, the photogenerated charges are separated at the Sb_2S_3 layer and not at the metal oxide/Sb_2S_3 interface, as in the case of TiO_2 /Sb_2S_3 interface. In reference to photogenerated charges separated at the TiO_2/ Sb_2S_3 interface, the electrons in the Sb_2S_3 are quenched by electron injection into TiO_2.[14] The TiO_2 density of states (DOS) is filled by the injected electrons; as a result, the photogenerated free electrons can be trapped in trap sites. This will add the TiO_2 states in the band gap to the Sb_2S_3 DOS, which will lower the electrons at the Fermi level and consequently will decrease the V_{oc}.[26] However, in the case of the Al_2O_3 or the ZrO_2, no states are added (since electron injection is not possible) so the V_{oc} will be higher.

In addition, it is important to mention the Sb_2S_3/P3HT interface, which is responsible for the interfacial hole transport. Charge separation occurs at the Sb_2S_3 layer (as stated earlier) in the Al_2O_3-based cells or the ZrO_2-based cells, although holes will transport through the P3HT hole conductor.

Figure 4b presents the external quantum efficiency (EQE) of the cells based on different metal oxides. The EQE spectra agree with the Sb_2S_3 and the P3HT absorption response, and its integration matches the current density observed by the solar simulator.

Figure 5 presents the histogram of the open circuit voltage of the solar cells prepared in this work: V_{oc} of 0.67 V for more than 20 Al_2O_3-based cells is shown in Figure 5; the average V_{oc} was 0.5 V for 13 TiO_2 cells; V_{oc} of 0.69 V is shown for 8 ZrO_2 cells, and V_{oc} over 0.71 V is shown for 6 ZrO_2 cells. In addition, the higher open circuit voltage achieved for the scaffold metal oxide Sb_2S_3-based solar cells compared to the TiO_2/Sb_2S_3-based solar cells is seen in the histogram. The higher V_{oc} observed for the ZrO_2-based cells compare to Al_2O_3-based cells can be attributed to lower recombination rate in the case of ZrO_2-based cells. The lower recombination rate in the case of the ZrO_2-based cells can be related to the difference in the isoelectric point. The ZrO_2 surface is more acidic than the Al_2O_3 surface, which is basic (according to the isoelectric point[27]). Therefore, it can be suggested that the acidic surface of the ZrO_2 is more suitable for the Sb_2S_3 growth, which results in less recombination and higher V_{oc}. Importantly, since the ZrO_2-based cells were not stable during the 3 h of the IMVS and IMPS measurements, it was difficult to extract the

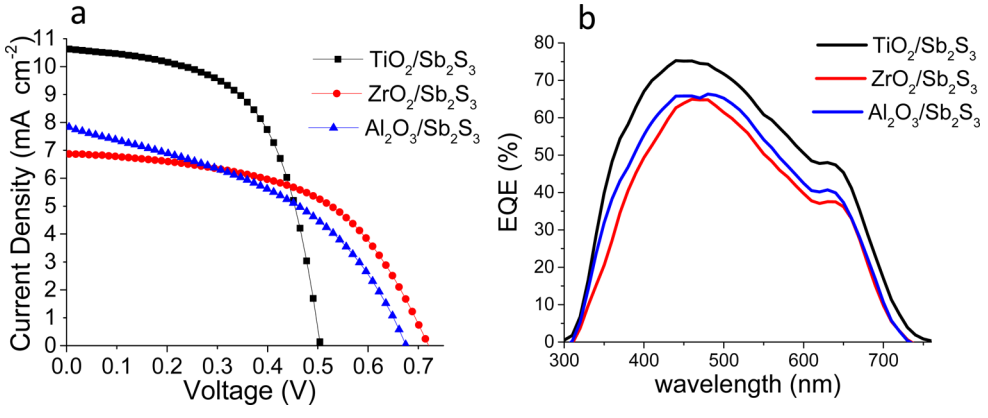

Figure 4. (a) Current voltage curves of the Al_2O_3/ Sb_2S_3, ZrO_2/ Sb_2S_3, and TiO_2/Sb_2S_3 solar cells. (b) Corresponding EQE spectra of the cells.

DOI: 10.1021/acs.jpcc.5b04231
J. Phys. Chem. C 2015, 119, 12904−12909

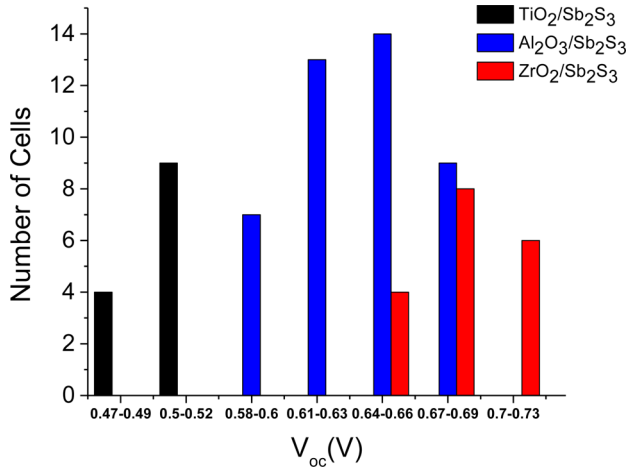

Figure 5. Histogram of the V_{oc} for the three metal oxides/Sb_2S_3 solar cells. The average and the standard deviation of the cells' V_{oc} are as follows: TiO_2 - V_{oc} = 0.47−0.49 V, average: 0.490 V ± 0.003; V_{oc} = 0.5−0.52 V, average: 0.505 V ± 0.007. Al_2O_3 - V_{oc} = 0.58−0.6 V, average: 0.601 V ± 0.006; V_{oc} = 0.61−0.63 V, average: 0.625 V ± 0.008; V_{oc} = 0.64−0.66 V, average: 0.655 V ± 0.009; V_{oc} = 0.67−0.69 V, average: 0.680 V ± 0.007. ZrO_2 - V_{oc} = 0.64−0.66 V, average: 0.663 V ± 0.004; V_{oc} = 0.67−0.69 V, average: 0.684 V ± 0.009; V_{oc} = 0.7−0.73 V, average: 0.715 V ± 0.011.

recombination rate of these cells, therefore more future study is required to elucidate the exact reason for the difference in V_{oc} between ZrO_2-based cells and Al_2O_3-based cells.

SEM cross section line scan of energy dispersive X-ray spectroscopy (EDS) was performed to clarify the reason for the PV performance of the Sb_2S_3 cells based on noninjected metal oxides (e.g., Al_2O_3 and ZrO_2). Figure 6a,b presents Al_2O_3/Sb_2S_3 and ZrO_2/ Sb_2S_3 HR-SEM cross sections, respectively, with the corresponding EDS line scan. In both panels, the components' concentration as a function of the thickness is clearly observed. The presence of S inside the mesoporous metal oxide film indicates that the Sb_2S_3 penetrates through the entire metal oxide film (e.g., Al_2O_3 and ZrO_2) which results in direct contact with the bottom electrodes. (The Sb was not detected due to difficulties detecting it in the EDS measurements.) This is certainly the main reason for the PV performance of these solar cell configurations.

In addition, IMVS and IMPS were performed to extract the electron diffusion length of the Sb_2S_3. The electron diffusion length (L_d) is calculated using the expression $L_d = d(\tau_r/\tau_t)^{1/2}$ (where d is the metal oxide thickness). The transport time (τ_t) is determined by the minimum frequency in IMPS spectra and the recombination lifetime (τ_r) is determined by the minimum frequency in IMVS spectra.[25] Both IMPS and IMVS spectra are measured at different light intensities, which correspond to different V_{oc}'s. The electron diffusion length is the length that electrons can travel without recombination; therefore, this parameter is extremely important for the solar cell operation. Long electron diffusion length can enhance the collection and light harvesting efficiency, which can improve the solar cell power conversion efficiency.

Figure 7 shows the electron diffusion length as a function of the voltage (light intensity) measured on Al_2O_3- and TiO_2-based solar cells. The electron diffusion length is in the range between 900 nm to 290 nm depending on the voltage for the Al_2O_3-based cells. As expected, the electron diffusion length decreased as the voltage increased. Two main conclusions can be extracted from this figure; (i) the electron diffusion length of the Al_2O_3/Sb_2S_3-based cells is longer than the electron diffusion length of the TiO_2/Sb_2S_3-based cells. This point supports the higher V_{oc} observed for the Al_2O_3-based cells. (ii) The measured electron diffusion length further supports the PV performance for the noninjected Sb_2S_3-based solar cells.

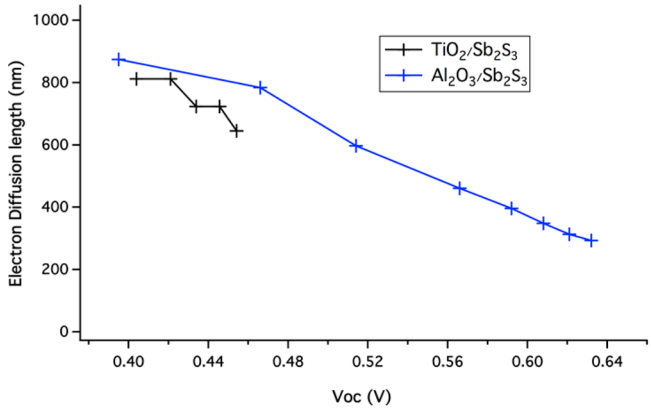

Figure 7. Electron diffusion length as a function of the voltage measured for the Al_2O_3/Sb_2S_3 and TiO_2/Sb_2S_3-based solar cells. The ZrO_2/Sb_2S_3-based cells were not stable during the 3 h of the IMVS and IMPS measurements.

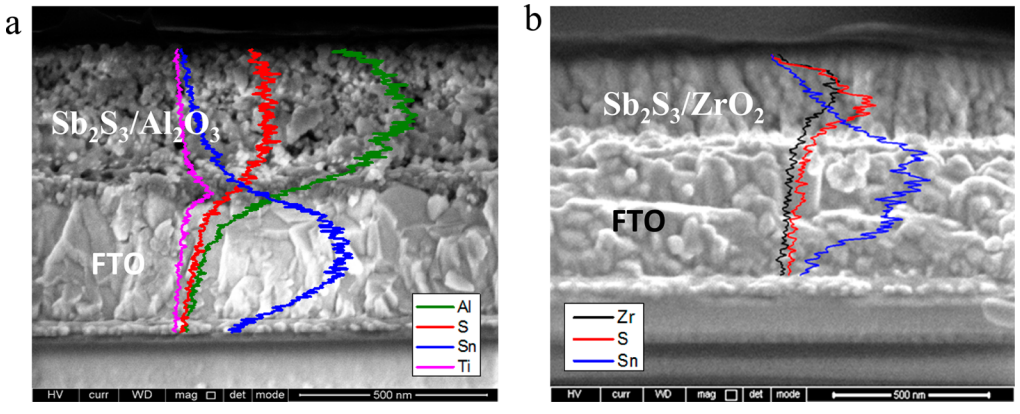

Figure 6. EDS line scan SEM cross-section images of (a) Sb_2S_3/Al_2O_3 and (b) Sb_2S_3/ZrO_2. The elements appear as different colors in the figure: S - sulfur, Al - Aluminum, Sn - Tin, Zr - Zirconium, Ti - Titanium. (The Ti element appeared in the blocking layer.).

DOI: 10.1021/acs.jpcc.5b04231
J. Phys. Chem. C 2015, 119, 12904−12909

CONCLUSIONS

In this work, Sb_2S_3 was grown on metal oxides (e.g., ZrO_2 or Al_2O_3) with a higher conduction band than the Sb_2S_3 conduction band, therefore electron injection was not possible. Surprisingly, this solar cell structure could work efficiently, achieving one of the highest V_{oc} (0.712 V) for Sb_2S_3-based solar cells. An EDS line scan revealed complete penetration of the Sb_2S_3 through the metal oxide pores. The long electron diffusion length measured by IMVS and IMPS techniques further supports operating of Sb_2S_3-based solar cells grown on metal oxide scaffold and justifies the higher open circuit voltage observed for the noninjected metal oxide-based solar cells. It can be concluded that when the photogenerated charges are separated at the Sb_2S_3 layer and not at the metal oxide/Sb_2S_3 interface (as in the case of TiO_2/Sb_2S_3 interface), it reduced the recombination and resulted in higher V_{oc} as in the case of noninjected metal oxide. This paper presents, for the first time, Sb_2S_3-based solar cells operated on scaffold metal oxide.

EXPERIMENTAL SECTION

Methods and Device Fabrication. *Device Fabrication.* The substrate of the device was a SnO_2:F(FTO) conducting glass (15 $\Omega \cdot cm^{-1}$, Pilkington). A blocking layer was deposited on the FTO glass using a solution of titanium diisopropoxidebis(acetylacetonate) (TiDIP, 75% in isopropanol, Aldrich) in ethanol (1:9 ratio). The TiDIP solution was spin coated at 2000 rpm and then annealed at 450 °C for 30 min. The TiO_2 paste was dissolved in ethanol at ratio of 1:3. The ZrO_2 and Al_2O_3 pastes were dissolved in isopropanol, at ratio of 1:12. The metal oxide nanoparticles solution was spin coated at 2000 rpm and annealed at 500 °C for 30 min subsequent to $TiCl_4$ (55 mM) treatment for 30 min at 70 °C and annealing at 500 °C for 30 min. The Sb_2S_3 layer was deposited by CBD with a solution of $SbCl_3$ and $Na_2S_2O_3$ as described in ref 13. The as-deposited orange films of amorphous Sb_2S_3 were annealed at 300 °C for 30 min under N_2 to give dark-brown crystalline stibnite. The cells were removed from the oven immediately after annealing and were allowed to cool under N_2. As an organic HTM, P3HT was used. The P3HT was prepared by spin coating 15 mg/mL in 1,2-dichlorobenzene solution with 2500 rpm for 60 s. Then, a layer of poly(3-4-ethylenedioxythiophene) with poly(4-stylenesulfonate) (PEDOT;PSS) was dissolved in methanol at a ratio of 1:2, and was spin-coated on the cells. The PEDOT:PSS/P3HT layers were annealed at 90 °C for 30 min under N_2. Finally, the back contact was deposited by evaporating 60 nm of silver under pressure of 5×10^{-6} Torr.

Photovoltaic Characterization. Photovoltaic measurements were made on a New Port system, composed of an Oriel I–V test station using an Oriel Sol3A simulator. The solar simulator was class AAA for spectral performance, uniformity of irradiance, and temporal stability. The solar simulator was equipped with a 450 W xenon lamp. The output power was adjusted to match AM1.5 global sunlight (100 mW cm^{-2}). The spectral match classifications were IEC60904-9 2007, JIC C 8912, and ASTM E927-05. I–V curves were obtained by applying an external bias to the cell and measuring the generated photocurrent with a Keithley model 2400 digital source meter. The voltage step and delay time of the photocurrent were 10 mV and 40 ms, respectively. Oriel IQE-200 was used to determine the monochromatic incident photon-to-electric current conversion efficiency. Under full computer control, light from a 150 W xenon arc lamp was focused through a monochromator in the 300–1800 nm wavelength range onto the photovoltaic cell under test. The monochromator was incremented through the visible spectrum to generate the IPCE (l) as defined by IPCE(l) = 12 400(J_{sc}/$l\varphi$), where l is the wavelength, J_{sc} is the short-circuit photocurrent density (mA cm^{-2}), and φ is the incident radiative flux (mW cm^{-2}). Photovoltaic performance was measured by using a metal mask with an aperture area of 0.09 cm^2.

Absorption Measurements. UV–vis absorption spectra measurements were performed using a Jasco V-670 spectrophotometer.

Ultra High Resolution Scanning Electron Microscopy (UHR-SEM) and Energy-dispersive X-ray spectroscopy (EDS). The images were obtained using Sirion UHR SEM of FEI (Field Emission Instruments, The Netherlands). The measurement conditions were 5 kV at various magnifications, as seen on the data bar of the images.

Intensity Modulated Photovoltage Spectroscopy (IMVS) and Intensity Modulated Photocurrent Spectroscopy (IMPS). The photocarrier recombination (transfer) times at open circuit (short circuit) were measured by IMVS (IMPS). The IMVS (IMPS) measurements were performed using an Autolab FRA32 M LED driver equipped with a red light source (627 nm), illuminating from the substrate side. The photovoltaic cells were illuminated with a bias light intensity with a sinusoidal wave modulation. The amplitude of the modulated photovoltage (photocurrent) density was kept at 10% or lower compared to the steady-state photovoltage (photocurrent) density, with frequencies ranging from 1 Hz to 20 kHz.

AUTHOR INFORMATION

Corresponding Author

*E-mail: lioz.etgar@mail.huji.ac.il.

Notes

The authors declare no competing financial interest.

ACKNOWLEDGMENTS

We are grateful for the financial support of Israel Alternative Energy Foundation (I-SAEF), the Ministry of Industry Trade and Labor Office of the Chief Scientist Kamin Project No. 50303, the Tashtiot project of the Office of the Chief Scientist, and the young German Israel foundation grant.

REFERENCES

(1) Tennakone, K.; Kumara, G. R. R.; Kottegoda, I. R. M.; Perera, V. S. P. An efficient dye-sensitized photoelectrochemical solar cell made from oxides of tin and zinc. *Chem. Commun.* **1999**, 15–16.

(2) Sayama, K.; Suguhara, H.; Arakawa, H. Photoelectrochemical Properties of a Porous Nb2O5 Electrode Sensitized by a Ruthenium Dye. *Chem. Mater.* **1998**, *10*, 3825–3832.

(3) Kuang, D.; Brillet, J.; Chen, P.; Takata, M.; Uchida, S.; Miura, H.; Sumioka, K.; Zakeeruddin, S. M.; Gratzel, M. Application of Highly Ordered TiO_2 Nsanotube Arrays in Flexible Dye-Sensitized Solar Cells. *ACS Nano* **2008**, *2* (6), 1113–1116.

(4) Grätzel, M. Dye-Sensitized Solar Cells. *J. Photochem. Photobiol.C: Photochem. Rev.* **2003**, *4*, 145–153.

(5) Kuang, D.; Ito, S.; Wenger, B. High Molar Extinction Co-Efficient Heteroleptic Ruthenium Complexes for Thin Film Dye- Sensitized Solar Cells. *J. Am. Chem. Soc.* **2006**, *128* (12), 4146–4154.

(6) Jiang, K. J.; Masaki, N.; Xia, J.-B.; Noda, S.; Yanagida, S. A Novel Ruthenium Sensitizer with a Hydrophobic 2-thiophen- 2-yl-vinyl-

DOI: 10.1021/acs.jpcc.5b04231
J. Phys. Chem. C 2015, 119, 12904–12909

Conjugated Bipyridyl Ligand for Effective Dye Sensitized TiO_2 Solar Cells. *Chem. Commun.* **2006**, *23*, 2460−2462.
(7) Wang, Z. S.; Sayama, K.; Sugihara, H. Efficient Eosin Y Dye-Sensitized Solar Cell Containing Br^-/Br^{-3} Electrolyte. *J. Phys. Chem. B* **2005**, *109* (47), 22449−22455.
(8) Sapp, S. A.; Elliott, C. M.; Contado, C.; Caramori, S.; Bignozzi, C. A. Substituted Polypyridine Complexes of Cobalt (II/III) as Efficient Electron-Transfer Mediators in Dye- Sensitized Solar Cells. *J. Am. Chem. Soc.* **2002**, *124* (37), 11215−11222.
(9) Oskam, G.; Bergeron, B. V.; Meyer, G. J.; Searson, P. C. Pseudohalogens for Dye-Sensitized TiO_2Photoelectrochemical Cells. *J. Phys. Chem. B* **2001**, *105* (29), 6867−6873.
(10) Sargent, E. H. Colloidal Quantum Dot Solar Cells. *Nat. Photonics* **2012**, *6*, 133−135.
(11) Kamat, P. V. Quantum Dot Solar Cells The Next Big Thing in Photovoltaics. *J. Phys. Chem. Lett.* **2013**, *4*, 908−918.
(12) Chang, J. A.; Rhee, J. H.; Im, S. H.; Lee, Y. H.; Kim, H. J.; Seok, S. I.; Nazeeruddin, M. K.; Grätzel, M. High-Performance Nanostructured Inorganic Organic Heterojunction Solar Cells. *Nano Lett.* **2010**, *10*, 2609−2612.
(13) Moon, S. J.; Itzhaik, Y.; Yum, J. H.; Zakeeruddin, S. M.; Hodes, G.; Grätzel, M. Sb_2S_3-Based Mesoscopic Solar Cell Using an Organic Hole Conductor. *J. Phys. Chem. Lett.* **2010**, *1*, 1524−1527.
(14) Snaith, H. J. Perovskites: The Emergence of a New Era for Low-Cost, High Efficiency Solar Cells. *Phys. Chem. Lett.* **2013**, *4*, 3623−3630.
(15) Graetzel, M. The Light and Shade of Perovskite Solar Cells. *Nat. Mater.* **2014**, *13*, 838−842.
(16) Fukumoto, T.; Moehl, T.; Niwa, Y.; Nazeeruddin, M. K.; Grätzel, M.; Etgar, L. Effect of Interfacial Engineering in Solid-State Nanostructured Sb_2S_3 Heterojunction Solar Cells. *Adv. Energy Mater.* **2013**, *3*, 29−33.
(17) Itzhaik, Y.; Niitsoo, O.; Page, M.; Hodes, G. Sb_2S_3-Sensitized Nanoporous TiO_2 Solar Cells. *J. Phys. Chem. C* **2009**, *113* (11), 4254−4256.
(18) HyukIm, S.; Lim, C. S.; Chang, J. A.; Lee, Y. H.; Mait, N.; Kim, H. J.; Nazeeruddin, Md. K.; Greatzel, M.; Seok, S. I. Toward Interaction of Sensitizer and Functional Moieties in Holetransporting Materials for Efficient Semiconductor-Sensitized Solar Cells. *Nano Lett.* **2011**, *11*, 4789−4793.
(19) Tsujimoto, K.; Nguyen, D. C.; Ito, S.; Nishino, H.; Matsuyoshi, H.; Konno, A.; Kumara, G. R. A.; Tennakone, K. TiO_2 Surface Treatment Effects by Mg^{2+}, Ba^{2+},and $Al3^+$ on Sb_2S_3 Extremely Thin Absorber Solar Cells. *J. Phys. Chem. C* **2012**, *116*, 13465−13471.
(20) Choi, Y. C.; Lee, D. U.; Noh, J. H.; Kim, E. K.; Seok, S. I. Highly Improved Sb_2S_3 Sensitized-Inorganic−Organic Heterojunction Solar Cells and Quantification of Traps by Deep-Level Transient Spectroscopy. *Adv. Funct. Mater.* **2014**, *24*, 3587−3592.
(21) Lee, M.; Teuscher, J.; Miyasaka, T.; Murakami, T. N.; Snaith, H. J. Efficient Hybrid Solar Cells Based on Meso-Superstructured Organometal Halide Perovskites. *Science* **2012**, *338*, 643−646.
(22) Messina, S.; Nair, M. T. S.; Nair, P. K. Antimony Sulfide Thin Films in Chemically Deposited Thin Film Photovoltaic Cells. *Thin Solid Films* **2007**, *515*, 5777−5782.
(23) O'Mahony, F. T. F.; Lutz, T.; Guijarro, N.; Gomez, R.; Haque, S. A. Electron and Hole Transfer at Metal Oxide/Sb_2S_3/spiro-OMeTADHeterojunctions. *Energy Environ. Sci.* **2012**, *5*, 9760−9764.
(24) Kralik, B.; Chang, E. K.; Louie, S. G. Structural Properties and Quasiparticle Band Structure of Zirconia. *Am. Phys. Soc.* **1998**, *57*, 7027−7036.
(25) Dymshits, A.; Rotem, A.; Etgar, L. High Voltage in Hole Conductor Free Organo-Metal Halide Perovskite Solar Cells. *J. Mater. Chem. A* **2014**, *2*, 20776−20781.
(26) Suarez, B.; Gonzalez-Pedro, V.; Ripolles, T. S.; Sanchez, R. S.; Otero, L.; Mora-Sero, I. Recombination Study of Combined Halides (Cl, Br, I) Perovskite Solar Cells. *J. Phys. Chem. Lett.* **2014**, *5*, 1628−1635.
(27) Zhang, Q.; Cao, G. Nanostructured photoelectrodes for dye-sensitized solar cells. *Nano Today* **2011**, *6*, 91−109.

DOI: 10.1021/acs.jpcc.5b04231
J. Phys. Chem. C 2015, 119, 12904−12909